Inorganic Chemistry

Article

pubs.acs.org/IC

Discovery of Spin Glass Behavior in $Ln_2Fe_4Sb_5$ (Ln = La–Nd and Sm)

W. Adam Phelan,[†] Giang V. Nguyen,[†] Jiakui K. Wang,[‡] Gregory T. McCandless,[†] Emilia Morosan,[‡] John F. DiTusa,[§] and Julia Y. Chan*[,†]

[†]Department of Chemistry, Louisiana State University, Baton Rouge, Louisiana 70803, United States

[‡]Department of Physics and Astronomy, Rice University, Houston, Texas 77005, United States

[§]Department of Physics and Astronomy, Louisiana State University, Baton Rouge, Louisiana 70803, United States

Supporting Information

ABSTRACT: Single crystals of $Ln_2Fe_4Sb_5$ (Ln = La–Nd and Sm) were grown from an inert Bi flux. Measurements of the single crystal X-ray diffraction revealed that these compounds crystallize in the tetragonal space group *I*4/*mmm* with lattice parameters of $a \approx 4$ Å, $c \approx 26$ Å, $V \approx 500$ Å^3, and $Z = 2$. This crystal structure consists of alternating $LnSb_8$ square antiprisms and Fe-sublattices composed of nearly equilateral triangles of bonded Fe atoms. These compounds are metallic and display spin glass behavior, which originates from the magnetic interactions within the Fe-sublattice. Specific heat measurements are void of any sharp features that can be interpreted as contributions from phase transitions as is typical for spin glass systems. A large, approximately linear in temperature, contribution to the specific heat of $La_2Fe_4Sb_5$ is observed at low temperatures that we interpret as having a magnetic origin. Herein, we report the synthesis, structure, and physical properties of $Ln_2Fe_4Sb_5$ (Ln = La–Nd and Sm).

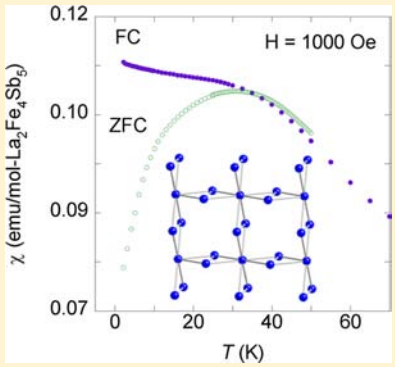

INTRODUCTION

Motivated by the diverse physical properties of ternary intermetallics with Group 15 elements such as As, Sb, and Bi, our research group and others have been involved in the discovery, synthesis, and structure determination of lanthanide-transition metal-pnictide compounds, such as the $LnTSb_3$ (Ln = early lanthanides; T = Ni, Fe, Co) phases.[1−8] These compounds are of particular interest because the number of transition metal analogues that can be synthesized allows for the investigation of the interplay of magnetism in both the lanthanide and transition metal sublattices. Many of these materials display local moment magnetism due to lanthanide ordering with no contribution from the transitional metal to the overall effective moment.[1−8] Similar behavior is also found in isostructural analogues of Ln_4FeGa_{12} (Ln = Tb, Dy, Ho, and Er) where the magnetic lanthanides order antiferromagnetically at temperatures below 25 K.[9] In contrast, the Y_4FeGa_{12} analogue orders ferromagnetically at 36 K with no localized magnetic moment on the Fe site so that the magnetism was attributed to the polarized itinerant electrons.[9]

Fe-containing intermetallics are well-known to exhibit interesting physical properties. For example, the new families of iron-based superconductors exhibit subtle structural transitions and antiferromagnetism as well as high superconducting transition temperatures. The superconductivity mechanism is not yet known but likely involves magnetic degrees of freedom.[10,11] The mechanism for the magnetism is not well understood in these complex materials but is likely tied to the Fermi surface geometry. More recently, a new iron pnictide compound, $CaFe_4As_3$, was reported, and unlike the layered, low-dimensional iron pnictide superconductors, the structure of $CaFe_4As_3$ is 3-dimensional.[12−14] Here, a second order incommensurate spin density wave transition at 88 K was clearly observed for $CaFe_4As_3$ in addition to a first order incommensurate to commensurate spin density wave transition observed at lower temperatures.[12,15,16] The higher temperature spin density wave order was shown to be very robust as chemical dopants and hydrostatic pressure had little effect on the ordering temperature. In contrast, the lower temperature first order incommensurate to commensurate spin density wave transition of $CaFe_4As_3$ was shown to be greatly influenced by these tuning parameters.[17] Investigations of the magnetism of the diverse set of iron pnictide compounds may be useful for understanding the complex magnetic behavior of the 2-D superconducting compounds.

Inspired by the first reported example of an $S = 1$ triangular system in $NiGa_2S_4$ ($FeGa_2S_4$-type),[18] we recently investigated a family of sulfides exhibiting magnetic frustration that results from an ordered triangular magnetic lattice. Studies of the isostructural analogues, MAl_2S_4 (M = Mn, Fe, and Co), led us to attribute the magnetic frustration observed in these compounds to a combination of geometric lattice frustration and magnetic site disorder.[19] Notably, the frustration factors (θ_w/T^*) for $FeGa_2S_4$[20] and $FeAl_2S_4$[19] were determined to be 10 ($\theta_w \approx -160$ K) and 21.4 ($\theta_w \approx -225$ K), respectively, indicative of a considerable degree of magnetic frustration.

With the goal of discovering compounds with the magnetism associated with the Fe-sublattice rather than simply from the lanthanide moments, we chose to grow single crystals of

Received: May 18, 2012
Published: October 24, 2012

   dx.doi.org/10.1021/ic301030f | *Inorg. Chem.* 2012, 51, 11412–11421

Table 1. Crystallographic Parameters for $Ln_2Fe_4Sb_5$ (Ln = La−Nd And Sm)

formula	$La_2Fe_{4.03}Sb_{4.94}$	$Ce_2Fe_{3.98}Sb_{4.93}$	$Pr_2Fe_{4.02}Sb_{4.93}$	$Nd_2Fe_{3.96}Sb_{4.91}$	$Sm_2Fe_{3.95}Sb_{4.93}$
a (Å)	4.3522(15)	4.3237(15)	4.3133(15)	4.3051(15)	4.2723(15)
c (Å)	26.201(8)	25.998(2)	25.976(15)	25.9080 (15)	25.558(9)
V (Å^3)	496.3(3)	486.0(2)	483.3(4)	480.2(2)	466.5(3)
Z	2	2	2	2	2
Crystal system	Tetragonal	Tetragonal	Tetragonal	Tetragonal	Tetragonal
Space group	$I4/mmm$	$I4/mmm$	$I4/mmm$	$I4/mmm$	$I4/mmm$
θ range (deg)	3.1−36.5	2.6−37.0	2.6−37.0	2.6−33.1	2.6−37.0
μ (mm^{-1})	27.24	28.26	29.15	29.87	32.23
			Data collection		
Crystal Size (mm)	0.01 × 0.08 × 0.10	0.03 × 0.05 × 0.08	0.03 × 0.08 × 0.10	0.01 × 0.08 × 0.13	0.03 × 0.10 × 0.13
Measured reflections	6672	6745	6743	5198	6413
Independent reflections	424	418	422	311	401
Reflections with $I > 2\sigma(I)$	398	375	392	298	384
R_{int}	0.028	0.025	0.030	0.026	0.031
h	0−7	0−7	0−7	0−6	0−7
k	−4→5	−4→5	−4→5	−3→4	−4→5
l	0−42	0−43	0−43	0−38	0−42
			Refinement		
$R_1[F^2 > 2\sigma(F^2)]^a$	0.046	0.038	0.049	0.044	0.040
$wR_2(F^2)^b$	0.121	0.104	0.149	0.118	0.111
Parameters	22	21	21	21	21
GOF	1.14	1.16	1.15	1.21	1.20
$\Delta\rho_{max}$ (e Å^{-3})	6.32	5.45	5.11	3.91	4.48
$\Delta\rho_{min}$ (e Å^{-3})	−2.71	−3.99	−3.28	−2.64	−5.70

$^aR_1=\sum||F_o| - |F_c||/\sum|F_o|$. $^bwR_2 = [\sum[w(F_o^2 - F_c^2)]/\sum[w(F_o^2)^2]]^{1/2}$.

$Ln_2Fe_4Sb_5$ (Ln = La−Nd and Sm) for these investigations. The synthesis and structure of $Ln_2Fe_4Sb_5$ (Ln = La−Nd) was first reported by P. Woll[21] and are structurally similar to the $LnTSb_3$ (Ln = early lanthanides; T = Ni, Fe, Co) phases.[1−8] However the physical properties of $Ln_2Fe_4Sb_5$ (Ln = La−Nd and Sm) largely remain uncharacterized. We have prepared single crystals of $Ln_2Fe_4Sb_5$ (Ln = La−Nd and Sm) in two ways; by direct reactions of the constituent elements as well as via an inert Bi flux. Spin glass features—most likely due to the Fe site disorder and the geometrical frustration inherent to this crystal structure—can be observed in the physical property data of $Ln_2Fe_4Sb_5$ (Ln = La−Nd and Sm). Because of the similarity of the magnetic susceptibility and magnetization of the La analogue to the other lanthanide containing analogues, we conclude that the spin glass state is associated with the Fe-sublattice in all of these materials. Herein, we report the synthesis, structure, physical properties, and structure−property relationships of $Ln_2Fe_4Sb_5$ (Ln = La−Nd and Sm).

EXPERIMENTAL SECTION

Synthesis. Small single crystals of $Ln_2Fe_4Sb_5$ (Ln = La−Nd and Sm) were first grown from a stoichiometric melt of the constituent elements. Ln = La−Nd, or Sm (3N − 99.9%), Fe (4N − 99.99%), and Sb (5N − 99.999%) were placed in separate 2 mL alumina crucibles in a 2:4:5 molar ratio of Ln: Fe: Sb. The crucibles were then sealed in separate evacuated fused-silica tubes and placed into a high temperature furnace. These reaction ampules were heated to 1200 °C for 24 h at a rate of 100 °C/h. The ampules were then cooled to 720 °C at a rate of 5 °C/h. Upon reaching 720 °C, the reaction ampules were taken from the furnace and allowed to cool on a benchtop. Small submilligram, plate-like crystals adequate for single crystal X-ray diffraction experiments were observed to grow in the shape of plates; however, larger crystals were needed for physical property measurements.

Our efforts to synthesize crystals suitable for physical property measurements led us to discover that larger (∼3 mm), single crystals of $Ln_2Fe_4Sb_5$ (Ln = La−Nd and Sm) could be grown *via* an inert Bi flux. Ln = La−Nd, and Sm (3N), Fe (4N), Sb (5N), and Bi (5N) were placed into separate 2 mL alumina crucibles in a 2:4:5:10 molar ratio of Ln/Fe/Sb/Bi. Each crucible was then topped with silica wool and sealed in separate evacuated fused-silica tubes and placed in a high temperature furnace. These reaction ampules were heated to 1200 °C for 72 h at a rate of 100 °C/h. The ampules were cooled to 825 °C at a rate of 5 °C/h, and the excess molten Bi flux was then separated from the plated-shaped single crystals via centrifugation.

Single-Crystal X-Ray Diffraction. Single crystals of $Ln_2Fe_4Sb_5$ (Ln = La−Nd and Sm) were mounted onto separate glass fiber tips of a goniometer using epoxy and placed on a Nonius KappaCCD X-ray diffractometer equipped with Mo Kα radiation (λ = 0.71073 Å). The crystallographic parameters for all compounds obtained from room temperature data collections are listed in Table 1. The tetragonal Laue symmetry $4/mmm$ and the observed systematic absences led to the space group selection of $I4/mmm$. The generation of the initial models and structure refinement were conducted using SIR97 and SHELX97, respectively.[22,23] After the refinement of all atomic positions, the collected data were corrected for extinction (SHELXL method) and absorption (multi-scan method).[23,24] The displacement parameters were then refined as anisotropic and weighting schemes were applied during the final stages of refinement. The atomic coordinates, displacement parameters, and occupancies are listed in Table 2. Selected interatomic distances and angles for all analogues are provided in Table 3. Since the reported compositions in Table 1 are very close to $Ln_2Fe_4Sb_5$ (Ln = La−Nd and Sm), the compounds hereafter will be referred to as $Ln_2Fe_4Sb_5$ (Ln = La−Nd and Sm).

Physical Properties. Magnetic data were collected using a Quantum Design Magnetic Property Measurement System (MPMS). The temperature-dependent magnetic susceptibility data were measured along the *a*- and *c*-axis of each crystal under an applied magnetic field of 1000 Oe under both zero-field cooled (ZFC) between 2.25 and 50 K and field cooled (FC) conditions between 2.25 and 400 K for all analogues. Field-dependent magnetization data were collected at 5 K with applied magnetic fields up to 5 T. The

dx.doi.org/10.1021/ic301030f | Inorg. Chem. 2012, 51, 11412−11421

Table 2. Atomic Coordinates, Anisotropic Displacement Parameters, and Occupancies for $Ln_2Fe_4Sb_5$ (Ln = La − Nd and Sm)

atom	Wyckoff site	x	y	z	U_{eq}(Å^2)[a]	occ.
La1	4*e*	0	0	0.34800(4)	0.0102(3)	1
Fe1	2*a*	0	0	0	0.0150(7)	1
Fe2	8*g*	0	1/2	0.45039(10)	0.0291(12)	0.759(14)
Sb1	4*d*	0	1/2	1/4	0.0088(3)	1
Sb2	4*e*	0	0	0.10768(4)	0.0104(3)	1
Sb3	8*j*	0	0.0788(11)	1/2	0.0298(17)	0.235(5)
Ce1	4*e*	0	0	0.34751(3)	0.0090(2)	1
Fe1	2*a*	0	0	0	0.0129(6)	1
Fe2	8*g*	0	1/2	0.44922(10)	0.0316(12)	0.744(12)
Sb1	4*d*	0	1/2	1/4	0.0070(2)	1
Sb2	4*e*	0	0	0.10983(4)	0.0091(2)	1
Sb3	4*e*	0	0	0.48595(15)	0.0412(13)	0.462(8)
Pr1	4*e*	0	0	0.34716(4)	0.0104(3)	1
Fe1	2*a*	0	0	0	0.0146(8)	1
Fe2	8*g*	0	1/2	0.44894(13)	0.0344(16)	0.755(19)
Sb1	4*d*	0	1/2	1/4	0.0085(3)	1
Sb2	4*e*	0	0	0.11072(5)	0.0100(4)	1
Sb3	4*e*	0	0	0.48405(18)	0.0318(13)	0.464(11)
Nd1	4*e*	0	0	0.34686(4)	0.0103(4)	1
Fe1	2*a*	0	0	0	0.0177(9)	1
Fe2	8*g*	0	1/2	0.44849(13)	0.0328(17)	0.739(17)
Sb1	4*d*	0	1/2	1/4	0.0080(4)	1
Sb2	4*e*	0	0	0.11160(5)	0.0100(4)	1
Sb3	4*e*	0	0	0.48338(16)	0.0247(13)	0.456(10)
Sm1	4*e*	0	0	0.34659(3)	0.0113(2)	1
Fe1	2*a*	0	0	0	0.0145(6)	1
Fe2	8*g*	0	1/2	0.44755(10)	0.0338(13)	0.737(13)
Sb1	4*d*	0	1/2	1/4	0.0097(2)	1
Sb2	4*e*	0	0	0.11287(4)	0.0109(3)	1
Sb3	4*e*	0	0	0.48335(12)	0.0240(9)	0.461(8)

[a] U_{eq} is defined as 1/3 of the trace of the orthogonalized U_{ij} tensor.

Table 3. Selected Interatomic Distances and Angles for $Ln_2Fe_4Sb_5$ (Ln = La−Nd and Sm)

	$La_2Fe_4Sb_5$	$Ce_2Fe_4Sb_5$	$Pr_2Fe_4Sb_5$	$Nd_2Fe_4Sb_5$	$Sm_2Fe_4Sb_5$
		Distance (Å)			
Ln−Sb1 (×4)	3.3657(10)	3.3318(8)	3.3197(15)	3.3062(10)	3.2645(10)
Ln−Sb2 (×4)	3.2893(11)	3.2522(11)	3.2403(12)	3.2288(12)	3.1937(11)
Fe1−Fe2 (×8)	2.5348(15)	2.5331(15)	2.5318(19)	2.5326(18)	2.5219(15)
Fe2−Fe2 (×1)	2.600(5)	2.641(5)	2.652(7)	2.669(6)	2.681(5)
Fe2−Sb2 (×2)	2.6553(18)	2.6514(18)	2.656(2)	2.657(2)	2.6360(17)
Fe2−Sb3 (×2)	2.247(4)−2.5579(17)	2.3634(19)	2.342(2)	2.335(2)	2.3239(17)
Sb1−Sb1 (×4)	3.0775(11)	3.0573(11)	3.0500(11)	3.0442(11)	3.0210(11)
		Angle (deg)			
Fe2−Fe1−Fe2	61.71(10)	62.83(10)	63.18(13)	63.59(13)	64.22(10)
Fe1−Fe2−Fe2	59.15(5)	58.59(5)	58.41(7)	58.20(6)	57.89(5)
Fe1−Fe2−Fe2	59.15(5)	58.59(5)	58.41(7)	58.20(6)	57.89(5)
Sb1−Sb1−Sb1	90.0	90.0	90.0	90.0	90.0

temperature dependent electrical resistivity and isothermal transverse magnetoresistance (MR) for $La_2Fe_4Sb_5$ and $Ce_2Fe_4Sb_5$ were measured by the standard four-probe ac-technique using the MPMS. The frequency and current employed for these experiments were 17 Hz and 1 mA, respectively. The specific heat capacity data for $La_2Fe_4Sb_5$ and $Ce_2Fe_4Sb_5$ were collected using a Quantum Design Physical Property Measurement System (PPMS).

RESULTS AND DISCUSSION

Structure. We first describe in detail the crystal structure of $La_2Fe_4Sb_5$ followed by a comparison of the other Ln analogues. The crystal structure of $La_2Fe_4Sb_5$ is shown in Figure 1. $La_2Fe_4Sb_5$ can be envisioned as being partially built from La1[$Sb1_4Sb2_4$] square antiprisms.[25] This subunit can be viewed in Figure 2a, and this network is also present in $LaSb_2$[26,27] and

dx.doi.org/10.1021/ic301030f | Inorg. Chem. 2012, 51, 11412−11421

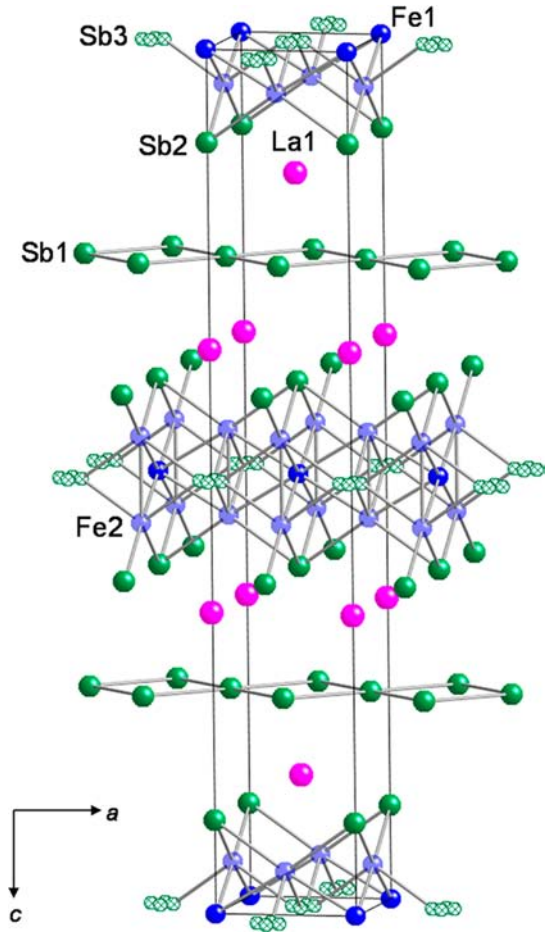

Figure 1. Crystal structure of $La_2Fe_4Sb_5$ with Fe2 and Sb3 represented by translucent blue sphere and green hatched spheres, respectively.

$LnTSb_3$ (Ln = early lanthanides; T = Cr, Ni, Fe, Co).[1−5,7,8,28,29] The La1 atoms are surrounded by 8 Sb atoms and adopt a square antiprismatic geometry. Four Sb1 atoms form a perfect square net and are situated directly above or below the La1 atoms, while four Sb2 atoms form a square directly below or above the La1 atoms but twisted 45° with respect to the perfect square net. The La−Sb bond distances of $La_2Fe_4Sb_5$ range from 3.2893(11)−3.3657(10) Å (Figure 2a) and are comparable to the La−Sb bond distances reported for $LaPdSb_3$ which also form square antiprisms (3.2850(5)−3.4252(17) Å).[3]

An expanded view of the Fe-sublattice for $La_2Fe_4Sb_5$ is shown in Figure 2b−d. The bonding interactions of Fe-sublattice can be partitioned into two parts (Fe−Sb and Fe−Fe bonds) which are shown in Figure 2b−c. The occupationally disordered Fe2 atoms (translucent blue spheres) are bonded to the Sb2 and Sb3 atoms in a tetrahedral arrangement as shown in Figure 2b. This arrangement is similar to the tetrahedral Fe−Pn coordination found in the new classes of iron pnictide superconductors[30,31] and the tetrahedral arrangement of the Ni−Sb bonds in $LnNi_{1-x}Sb_2$ (Ln = Y, Gd−Er).[32] Fe2−Sb2 and Fe2−Sb3 bond distances correspond to 2.6553(18) and 2.247(7)−2.5579(17) Å, respectively. These Fe2−Sb3 bond distance are smaller than the Fe−Sb bond distances of $FeSb_2$, which range from 2.5762(6)−2.6164(11) Å.[33,34] Similar short interatomic distances were observed for $La_2Fe_{5-x}Sb_{10-y}$ (x = 1.12, y = 5.08) and were attributed to the occupational disorder of the Fe2 position.[25] The positional disorder of the Sb3 position for $La_2Fe_4Sb_5$ also influences the short Fe2−Sb3 interatomic distances as the elongated Fe2 anisotropic displacement parameters point the in direction of the Sb3 positions. The Fe−Fe contacts within the Fe-sublattice of $La_2Fe_4Sb_5$ are shown in Figure 2c and form a 2-dimensional bowtie network of Fe−Fe bonds composed of nearly equilateral triangles. The triangles are comprised of Fe1 atoms (blue spheres) bonded to two Fe2 atoms (translucent blue spheres) at a distance of 2.5348(15) Å, and an Fe2−Fe2 bond at a distance of 2.600(5) Å. These Fe−Fe bond distances are slightly smaller than the Fe−Fe bond distances reported for the $LnFeSb_3$ (Ln = Pr, Nd, Sm, Gd, and Tb) compounds where 2.683(2) Å is the measured Fe−Fe bond distance for $PrFeSb_3$.[7] The nearly equilateral triangles of Fe and the occupational disorder modeled for the Fe2 site present the possibility for geometric magnetic frustration and associated spin glass ordering in $Ln_2Fe_4Sb_5$ (Ln = La − Nd and Sm).[35] The physical properties presented below do indeed exhibit features inherent to many spin-glass systems. Figure 2d shows the complete bond arrangement of the Fe-sublattice of $La_2Fe_4Sb_5$.

There are some subtle differences across this series of compounds in the positional disorder we observe. For example the positional disorder for Sb3 varies from $La_2Fe_4Sb_5$ as compared to $Ln_2Fe_4Sb_5$ (Ln = Ce − Nd and Sm), as this position is slightly shifted in a different manner from the 2*b* Wyckoff position which has the Wyckoff site symmetry of 4/*mmm*. A large, unrealistic U_{eq} value for Sb3 in all analogue models results when this atom is left on the 2*b* Wyckoff position. The Sb3 position for $La_2Fe_4Sb_5$ is positionally disordered around a 4-fold axis of rotation whereas, the Sb3 position for $Ln_2Fe_4Sb_5$ (Ln = Ce−Nd and Sm) is positionally disordered around a mirror plane. P. Woll also observed that the Sb3 position of $Ce_2Fe_4Sb_5$ and $Pr_2Fe_4Sb_5$ were positionally disordered around a mirror plane; however, no positional disorder was modeled for the Sb3 position of $La_2Fe_4Sb_5$ or $Nd_2Fe_4Sb_5$.[21] Modeling the positional disorder of the Sb3 for $La_2Fe_4Sb_5$ and $Nd_2Fe_4Sb_5$ as described above was found to be more suitable. The positional disorder of the Sb3 positions for these materials is unusual compared to other disordered Sb-containing materials. For example, the observed disorder in the $Hf_{10}M_xSb_{6-x}$ compounds was modeled as occupationally disordered, where the Sb and M atoms share the same site.[36] However, while the Sb deficiencies exhibited by $Ln_2Fe_4Sb_5$ (Ln = Ce−Nd and Sm) are somewhat rare, these deficiencies have been previously identified by P. Woll[21] and Nasir et al.[25]

The Sb2 atoms which form the square nets in $La_2Fe_4Sb_5$ are separated by a distance of 3.0775(11) Å. These planar square Sb sheets are commonly observed geometric networks in Sb-containing compounds.[37,38] A bond distance of 3.0775(11) Å is slightly larger but comparable to the Sb−Sb bond distances reported for $LnFeSb_3$ (Ln = Pr, Nd, Sm, Gd, and Tb) (~3.00 Å)[7] and those reported for the Zintl phase Sr_2Sb_3 (2.887−2.922 Å).[39] However, these Sb−Sb distances are shorter than those reported for $Eu_{14}MnSb_{11}$ (3.258(2) Å).[40]

Physical Properties. The temperature-dependent magnetic susceptibility for $La_2Fe_4Sb_5$ is shown in Figure 3. Here a magnetic field of 1000 Oe was applied along the *a*- (open circles) and *c*-axes (closed circles) of the crystal. For each of these data sets a broad maximum is apparent near $T^* \approx 30$ K below which the field cooled (FC) and zero field cooled (ZFC) data are substantially different. Above T^* the magnetic susceptibility resembles a Curie−Weiss like form indicative of a paramagnetic state. These same general features can be

dx.doi.org/10.1021/ic301030f | *Inorg. Chem.* 2012, 51, 11412−11421

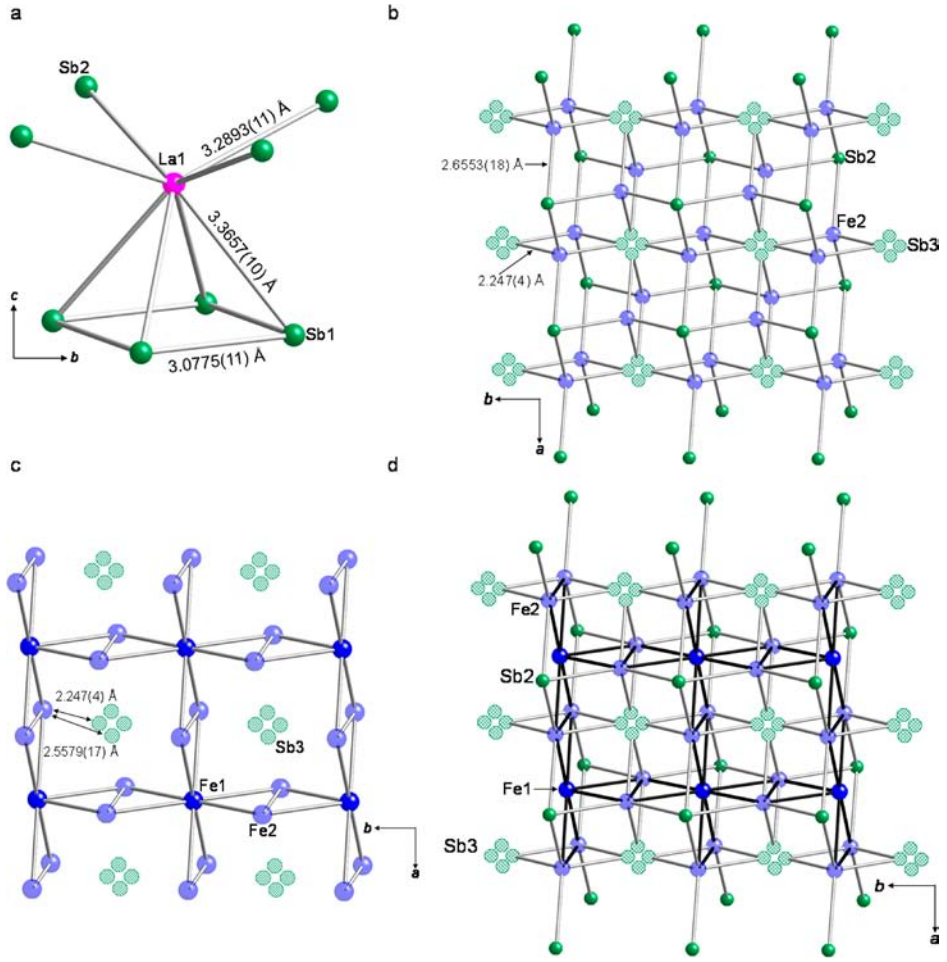

Figure 2. (a–d) Structural subunits comprising $La_2Fe_4Sb_5$.

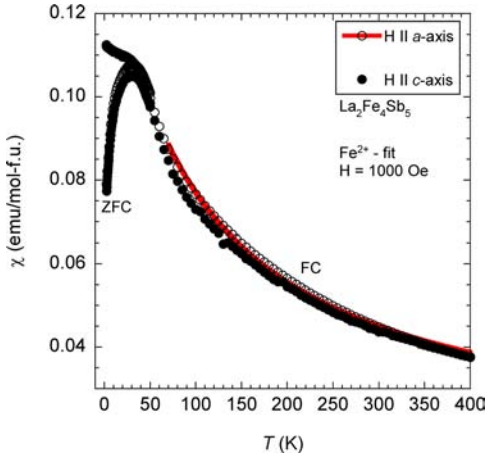

Figure 3. Temperature-dependent magnetic susceptibility (χ) for $La_2Fe_4Sb_5$ where a magnetic field (H) of 1000 Oe was applied along the *a*- and *c*-axes of the crystal.

observed in Figure 4 where the magnetic susceptibility of each of the lanthanide analogues investigated in this study is presented. Although there is some variation in the magnitude of χ, Figures 3 and 4 demonstrate that the magnetic response of these materials does not dramatically change upon variation of the Ln element. These observations indicate that the magnetic susceptibility of these compounds is dominated by the Fe-sublattice rather than by the lanthanide ions. In addition, there is only a moderate anisotropy in the magnetic susceptibility of these compounds, reflecting the anisotropy of the crystalline lattice. Our magnetization measurements as a function of field taken at 5 K, a temperature well below T^*, are displayed in Figure 5 where only a small hysteresis compatible with our FC and ZFC susceptibility data is observed. We conclude from these observations that the low temperature magnetic state of all of these compounds is most likely that of a spin glass. This magnetic behavior correlates well with the structural motif shown in Figure 2c, where the nearly equilateral triangles composed of magnetic Fe-ions combined with the occupational disorder of the Fe2 and the positional disorder of the Sb3 site can most certainly lead to spin glass behavior.[35] Similar to the spin glass materials MAl_2S_4 (M = Mn, Fe, and Co),[19] the spin glass behavior of $Ln_2Fe_4Sb_5$ (Ln = La–Nd and Sm) results from the magnetic interactions of an occupationally disordered transition metal sublattice.

A more quantitative accounting of our magnetic susceptibility data was carried out by comparing the Curie–Weiss form, $\chi(T) = \chi_0 + C/(T - \theta_w)$, where C represents the Curie constant, θ_w denotes the Weiss temperature, and χ_0 represents the temperature-independent contributions to the magnetic susceptibility due to Larmor diamagnetism and Pauli paramagnetism, to our $La_2Fe_4Sb_5$ data. When we performed fits of this form to the data taken with H|| crystalline *a*-axis with the Curie constant as a free parameter, we find that C is not well determined by the data above 70 K as $\chi(T)$ does not vary over

dx.doi.org/10.1021/ic301030f | *Inorg. Chem.* 2012, 51, 11412–11421

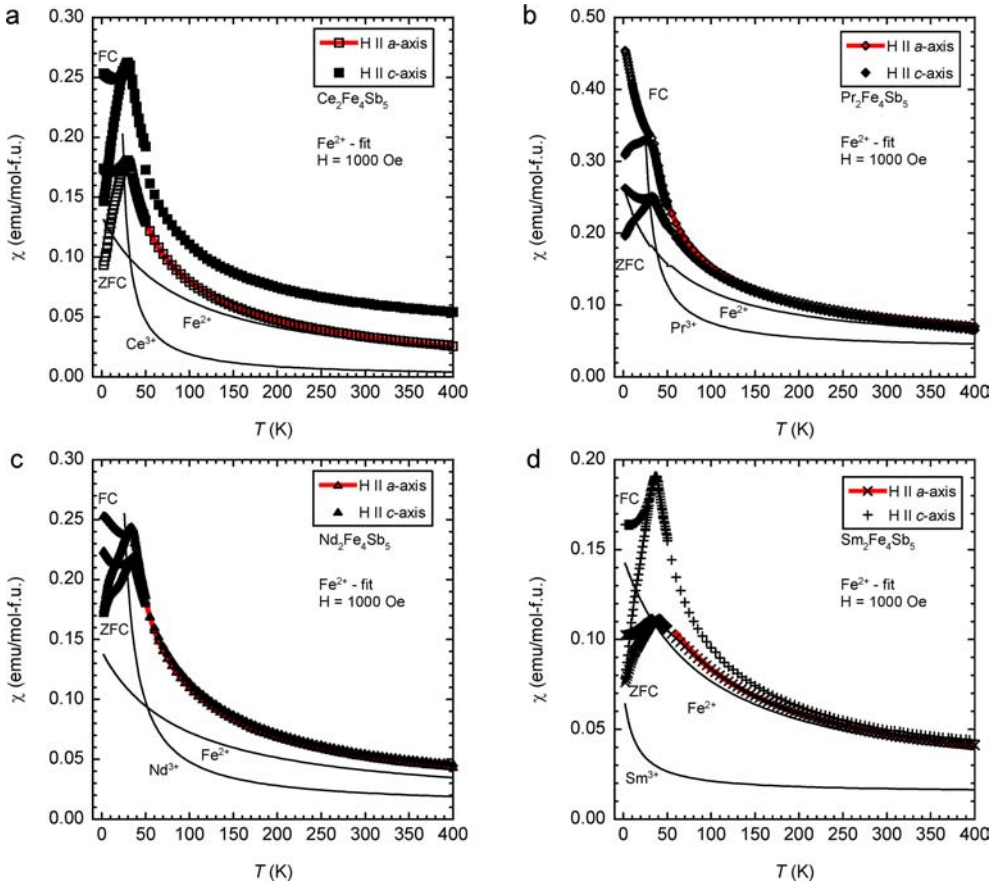

Figure 4. (a–d) Temperature-dependent magnetic susceptibility (χ) of $Ln_2Fe_4Sb_5$ (Ln = Ce − Nd, and Sm) where a magnetic field (H) of 1000 Oe was applied along the *a*- and *c*-axes of the crystal structure.

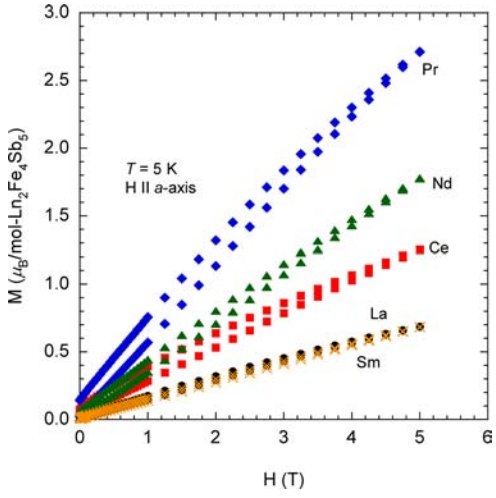

Figure 5. Field-dependent magnetization (M) of $Ln_2Fe_4Sb_5$ (Ln = La–Nd, and Sm) where magnetic fields up to 5 T were applied along the *a*-axis of the crystal structure at 5 K.

a wide enough range to fully constrain the 3 parameters in the above expression. Therefore, we performed fits with the Curie constant fixed at the expected values for Fe^{2+} and Fe^{3+}. The usual form,

$$C = \frac{N_A \times g^2 \times \mu_B{}^2 \times J(J+1)}{3k_B} = \frac{N_A \times p_{eff}^2}{3k_B} \quad (1)$$

was used to calculate the expected Curie constant for both an Fe^{2+} and Fe^{3+}-sublattice in $La_2Fe_4Sb_5$. Here N_A is Avogadro's number, g is the Landé g-factor, μ_B is the Bohr magneton, J is the total angular momentum as predicted by Hund's rules, and k_B is Boltzmann's constant.[41] The Curie constant values which correspond to an Fe^{2+} and Fe^{3+}-sublattice for $La_2Fe_4Sb_5$ were calculated to be 12.094 cm^3 K/mol and 17.638 cm^3 K/mol, respectively. This form was fit to the magnetic susceptibility data for $La_2Fe_4Sb_5$ from 70 to 400 K by setting the Curie constant equal to the calculated values and allowing θ_w and χ_0 to float. The best fit magnetic parameters assuming an Fe^{2+} model obtained from this procedure are listed in Table 4, and the resulting fit along the *a*-axis is shown in Figure 3. (The best

Table 4. Magnetic Parameters for $La_2Fe_4Sb_5$

	Fe^{2+} − fit
H‖*a*-axis	
Fit Region	70–400 K
χ_0 (emu/mol-f.u.)	0.01422(2)
C (cm^3 K/mol)	12.094
θ_w	−92.7(9)
R^2	0.99716
H‖ *c*-axis	
Fit Region	60–400 K
χ_0 (emu/mol-f.u.)	0.0139(1)
C (cm^3 K/mol)	12.094
θ_w	−101.6(6)
R^2	0.99862

dx.doi.org/10.1021/ic301030f | Inorg. Chem. 2012, 51, 11412–11421

Table 5. Magnetic Parameters for $Ln_2Fe_4Sb_5$ (Ln = Ce−Nd and Sm) with H|| *a*-Axis

	$Ce_2Fe_4Sb_5$	$Pr_2Fe_4Sb_5$	$Nd_2Fe_4Sb_5$	$Sm_2Fe_4Sb_5$
Fit Region	45−400 K	37.5−400 K	40−400 K	60−400 K
χ_0 (emu/mol-f.u.)	−0.0028(5)	0.0378(2)	0.01056(6)	0.0146(2)
C_{Fe2+} (cm^3 K/mol)	11.944	12.064	11.884	11.854
C_{Ln3+} (cm^3 K/mol)	1.599	3.201	3.271	0.757
θ_{Fe2+} (K)	−89.1(4)	−53.5(8)	−91.5(4)	−90.5(3)
θ_{Ln3+} (K)	16.1(2)	14.6(3)	12.6(1)	13(11)
R^2	0.99995	0.99970	0.99996	0.99873

Table 6. Magnetic Parameters for $Ln_2Fe_4Sb_5$ (Ln = Ce−Nd and Sm) with H|| *c*-Axis

	$Ce_2Fe_4Sb_5$	$Pr_2Fe_4Sb_5$	$Nd_2Fe_4Sb_5$	$Sm_2Fe_4Sb_5$
Fit Region	45−400 K	37.5−400 K	40−400 K	60−400 K
χ_0 (emu/mol-f.u.)	0.0250(3)	0.0329(5)	0.0127(9)	0.01566(1)
C_{Fe2+} (cm^3 K/mol)	11.944	12.064	11.884	11.854
C_{Ln3+} (cm^3 K/mol)	1.599	3.201	3.271	0.757
θ_{Fe2+} (K)	−91(2)	−38(5)	−74.5(6)	−76.0(9)
θ_{Ln3+} (K)	27.0(3)	−16(11)	4.3(2)	37.2(6)
R^2	0.99833	0.99746	0.99992	0.99933

fit magnetic parameters assuming an Fe^{3+} model obtained using a similar fitting procedure are listed in Supporting Information Table S1, and the resulting fit along the *a*-axis is shown in Figure S1 of the Supporting Information) From Figures 3 and S1 and Tables 4 and S2, we observe that the Fe^{2+} and Fe^{3+} models fit the data almost equally well. Therefore, it is not possible to reliable assign the oxidation state of the Fe species in this compound using this simple fitting procedure. However, the divergence of the field cooled (FC) and zero-field cooled (ZFC) magnetic susceptibility around $T^* \approx 30$ K and the large Weiss temperature of $\theta_w \approx -100$ K ($\theta_w \approx -150$ K) inferred from the Fe^{2+} (Fe^{3+}) fits along both axes support the notion of a low temperature spin glass state in $La_2Fe_4Sb_5$ originating in the Fe-sublattice.

We have also considered an averaged susceptibility, $\chi_{ave} = (1/3)(2\chi_a + \chi_c)$, in order to reduce the effects of any possible crystal field splitting on the susceptibility data. The values of the fit parameters were found to interpolate well between our *a*- and *c*-axes fitting parameters, and all of our previous conclusions were verified for this averaged data.

After characterizing the La compound, we explored the changes that occur upon substituting Ln elements on the La site expecting more complex magnetic behavior. However, the magnetic susceptibility are not vastly different across the series as can be seen in Figure 4a-d where the data for $Ln_2Fe_4Sb_5$ (Ln = Ce−Nd and Sm) in a magnetic field of 1000 Oe applied along the *a*- (open symbols) and *c*-axes (closed symbols) of the crystals are displayed. When a similar fitting procedure to that described above was employed to fit these data, we did not find satisfactory convergence of eq 1. This model assumes a single magnetic moment results from both the Ln and the Fe sublattices. Thus the data forced us to consider a slightly more complex model where we considered the Fe and Ln ions to form two noninteracting magnetic sublattices. Here we used a Curie−Weiss equation with the inclusion of a second Curie−Weiss term, $\chi(T) = \chi_0 + C_{Fe2+}/(T - \theta_{Fe2+}) + C_{Ln3+}/(T - \theta_{Ln3+})$. The expected Curie constants for an independent Fe^{2+}-sublattice and Ln^{3+} (Ln^{3+} = Ce^{3+}−Nd^{3+} and Sm^{3+}) sublattice were calculated using eq 1 and are displayed in Table 5 and Table 6 for the *a*- and *c*-axes, respectively. The magnetic susceptibility data for $Ln_2Fe_4Sb_5$ (Ln = Ce−Nd and Sm) were fit by setting the two Curie constants equal to the calculated values Fe^{2+} and Ln^{3+} (Ln^{3+} = Ce^{3+}−Nd^{3+} and Sm^{3+}) and allowing the θ_w and χ_0 parameters to float. The results of these fits along the *a*-axis are shown in Figure 4a−d. (Similar fits were performed to the same data where an independent Fe^{3+}-sublattice and Ln^{3+} (Ln^{3+} = Ce^{3+}−Nd^{3+} and Sm^{3+}) sublattice were calculated using eq 1. The results of these fits along the *a*-axis are shown in Supporting Information Figure S2a−d. The parameters obtained from these fits can be viewed in Tables S2 and S3 for the *a*- and *c*-axes, respectively, in the Supporting Information section.) Lines which correspond to the calculated magnetic susceptibility based on these parameters for the individual Ln^{3+} and Fe^{2+}-sublattice contributions along the *a*-axis for $Ln_2Fe_4Sb_5$ (Ln = Ce−Nd and Sm) are included in Figure 4a−d. Our best fits that result from the procedure described above are dominated above 100 K by the contribution from the Fe-sublattice which is very similar in magnitude to that found in the La compound. An additional contribution dominates in a narrow temperature range above T^*. The observed large increase in $\chi(T)$ at temperatures above T^* result in positive Weiss temperatures ($\theta_{Ln3+} > 0$), which alone suggests ferromagnetic interactions within the Ln-sublattice. The small changes in the magnetic susceptibility for $T > 100$ K along with the quality of the fits of this simple model to the data support the notion that the Ln^{3+} and Fe^{2+}- or Fe^{3+}-sublattices are not well coupled to one another in this *T*-range. Additionally, the divergence of the field cooled (FC) and zero-field cooled (ZFC) magnetic susceptibility around 30 K ($T^* \approx 30$ K) and the large negative θ_w evidence low temperature spin glass behavior for all $Ln_2Fe_4Sb_5$ (Ln = Ce−Nd and Sm) crystals investigated. Such a divergence in the FC and ZFC concomitant with a large negative θ_w is indicative of spin glass behavior as highlighted by Ramirez.[35]

Little to no magnetic anisotropy is observed in the magnetic data and fit parameters when the susceptibilities for $Ln_2Fe_4Sb_5$ (Ln = La, Ce, and Nd) are compared along the different axial directions. However, some magnetic anisotropy is observed in the magnetic data when the magnetic susceptibilities for $Pr_2Fe_4Sb_5$ and $Sm_2Fe_4Sb_5$ are compared along the different axial directions and when the fit parameters from Tables 5 and 6 are compared. Therefore, we conclude the Pr^{3+} and the Sm^{3+}

magnetic sublattices are somewhat more anisotropic than the other Ln magnetic sublattices but that the ordering temperatures and the history dependence are not greatly affected.

The field-dependent magnetization up to 5 T at 5 K is presented in Figure 5 for $Ln_2Fe_4Sb_5$ (Ln = La−Nd and Sm) with the magnetic field applied along the *a*-axis of these crystals. The small hysteresis effects for each analogue mentioned above are also indicative of spin glass behavior. Spin glass materials are characterized by their large number of nearly degenerate states, therefore, the exact ground states occupied at low temperatures is determined by the history of the experimental conditions and thus irreversible magnetic behavior is observed.[35]

The electrical resistivity versus temperature for $La_2Fe_4Sb_5$ and $Ce_2Fe_4Sb_5$ is shown in Figure 6. Both analogues display

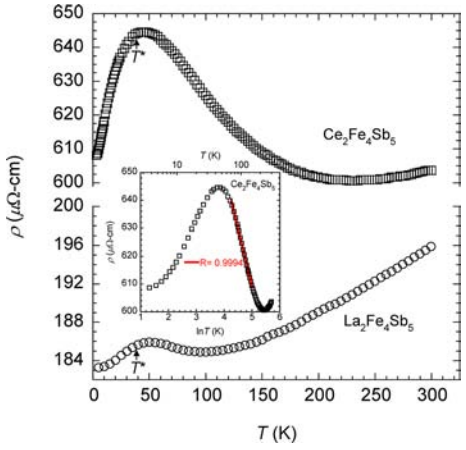

Figure 6. Temperature dependent electrical resistivity (ρ) for $La_2Fe_4Sb_5$ and $Ce_2Fe_4Sb_5$. The inset shows a liner fit to the resistivity (ρ) vs ln$T$ of $Ce_2Fe_4Sb_5$ from 70 to 150 K.

metallic behavior down to 3 K. $La_2Fe_4Sb_5$ and $Ce_2Fe_4Sb_5$ both display a wide range of temperatures where ρ decreases with T, between 50 and 100 K for $La_2Fe_5Sb_5$ and between 50 and 225 K for $Ce_2Fe_4Sb_5$. A Kondo mechanism is usually suspected when $d\rho/dT < 0$ over wide ranges of temperature in metallic systems containing magnetic moments, and a plot of ρ as a function of ln$T$ for $Ce_2Fe_4Sb_5$ is included in the inset of Figure 6 for a comparison to the usual Kondo form. A similar linear fit ρ vs ln$T$ curve in the region of the upturn for $La_2Fe_4Sb_5$ is not displayed due to the limited temperature range where $d\rho/dT < 0$. In addition, resistivity maxima are observed close to $T^* \approx 30$ K where the bifurcations were observed in the ZFC and FC magnetic susceptibility data for both $La_2Fe_4Sb_5$ and $Ce_2Fe_4Sb_5$. Below T^* the resistivity decreases slightly so that these curves resemble traditional spin glass systems where an incoherent Kondo regime is present above a glassy freezing temperature (T^*). Below (T^*) the Ruderman-Kittel-Kasuya-Yosida (RKKY) interactions become important and serve to "freeze out" the spins fluctuations reducing the spin disorder scattering.[42]

The magnetoresistance as a function of an applied magnetic field at various temperatures for $La_2Fe_4Sb_5$ and $Ce_2Fe_4Sb_5$ is shown in Figure 7a−b. The magnetoresistance for both compounds is small and positive for all temperatures and fields measured with the exception of the low field values at T = 250 and 300 K for $Ce_2Fe_4Sb_5$. The origin of this positive magnetoresistance is unknown, as Kondo systems typically exhibit negative magnetoresistances.[43] However, the structurally related $LnNi(Sn,Sb)_3$ (Ln = Pr, Sm, Gd, and Nd) compounds also exhibit small positive magnetoresistance values at 3 K.[5]

The specific heat of $Ln_2Fe_4Sb_5$ (Ln = La and Ce) is shown in Figure 8. From the inset of this figure, it can be observed that no thermodynamic phase transitions are present down to the lowest temperatures measured, although a small anomaly can be observed near T^* for $Ce_2Fe_4Sb_5$. The simultaneous occurrence of sharp ordering features in the magnetic response and the absence of a response in the thermal properties is consistent with glassy order.[35] A plot of the specific heat divided by temperature (C_p/T) as a function of T^2 for $Ln_2Fe_4Sb_5$ (Ln = La and Ce) is shown in Figure 9. Again, no thermodynamic phase transitions are visible in this plot, although the small anomaly around 35 K observed for the Ce compound suggests a small gain in the magnetic entropy near T^*. Fits of the C_p/T vs T^2 data to the standard metallic form ($C_p = \gamma T + \beta T^3$) were performed in order to determine the γ and β coefficients for $La_2Fe_4Sb_5$. The values these coefficients for the best fits to our $La_2Fe_4Sb_5$ data were found to be 118 mJ/mol-$La_2Fe_4Sb_5$ K^2 and 2.85 mJ/mol-$La_2Fe_4Sb_5$ K^4, respectively.

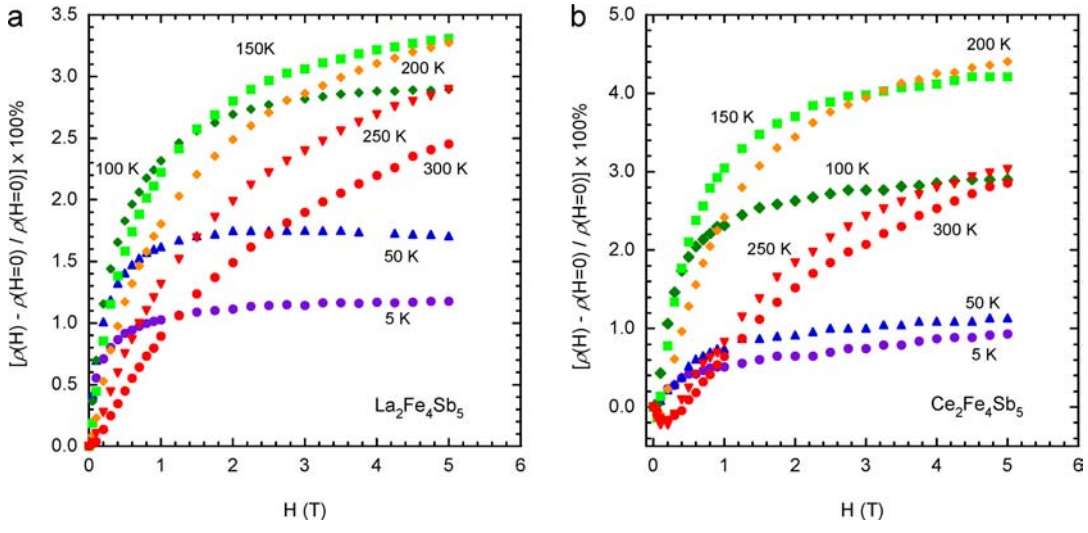

Figure 7. Field dependent magnetoresistance $[(\rho(H) - \rho(H = 0)/\rho(H = 0)) \times 100\%]$ for (a) $La_2Fe_4Sb_5$ and (b) $Ce_2Fe_4Sb_5$ at various temperatures.

dx.doi.org/10.1021/ic301030f | *Inorg. Chem.* 2012, 51, 11412−11421

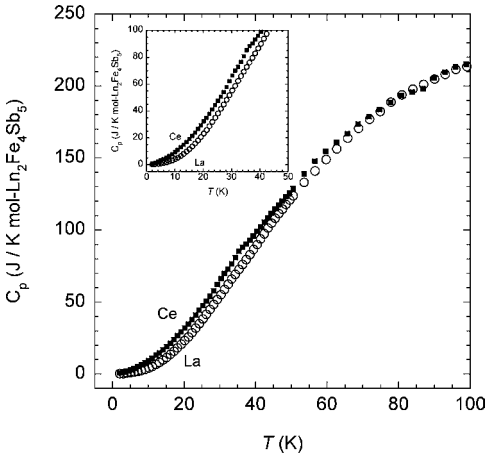

Figure 8. Specific heat capacity (C_p) for $La_2Fe_4Sb_5$ and $Ce_2Fe_4Sb_5$ as a function of temperature.

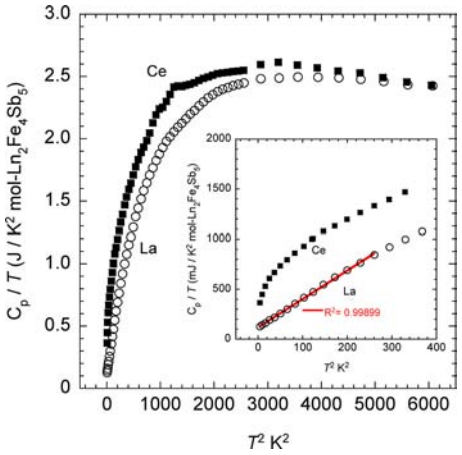

Figure 9. Specific heat capacity divided by temperature (C_p/T) of $La_2Fe_4Sb_5$ and $Ce_2Fe_4Sb_5$ as a function of temperature squared (T^2).

Even when accounting for the larger number of elements per formula unit in $La_2Fe_4Sb_5$, this value is substantially larger than found in simple metals like like Cu, which has a $\gamma \approx 0.7$ mJ/mol K^2.[44] A similar fit to the C_p/T vs T^2 data for $Ce_2Fe_4Sb_5$ appears not to be appropriate since the data do not resemble this simple form. We believe that contributions from the magnetic degrees of freedom associated with the Ce *f*-electrons is significant in this *T*-range and an accurate separation of magnetic, electronic, and phonon contributions was not deemed possible.

CONCLUSION

Single crystals of $Ln_2Fe_4Sb_5$ (Ln = La−Nd and Sm) were grown using an inert Bi flux. Single crystal X-ray diffraction experiments revealed Fe−Sb bonds that form a tetrahedral arrangement similar to that found in the new classes of iron pnictide superconductors.[30,31] This tetrahedral PbO-type slab is not seen in the early lanthanide-transition metal-antimonides previously studied (e.g., $LnTSb_3$ (Ln = early lanthanides; T = Ni, Fe, Co)[1−8]) but instead observed in the late lanthanide-transition metal-antimonides (e.g., $LnNi_{1-x}Sb_2$ (Ln = late lanthanide)).[8,32] We have shown by way of the similarity in the magnetic response of the La compared to the Ce − Nd and Sm compounds that the spin-glass behavior of $Ln_2Fe_4Sb_5$ (Ln = La−Nd and Sm) results from magnetic correlations within the Fe-sublattices. The Fe−Fe bonding structural motif of the Fe-sublattices correlates well with the glassy magnetic properties presented for each analogue. The resistivity and heat capacity measurements of $La_2Fe_4Sb_5$ and $Ce_2Fe_4Sb_5$ further support the spin glass behavior in these compounds. The origin of the large Sommerfeld (γ = 118 mJ/mol-$La_2Fe_4Sb_5$ K^2) coefficient determined from fits to the heat capacity of $La_2Fe_4Sb_5$ is unknown. A similar but larger effect in the geometrically frustrated spinel, LiV_2O_4, has been attributed to heavy-fermion behavior.[45] The origin of enhanced mass behavior in LiV_2O_4 is thought to be different from the traditional heavy-fermion mechanism in Ce, Yb, and U-containing compounds. Instead, the origins of heavy-fermion behavior in LiV_2O_4 has been attributed to geometric frustration.[45] We cannot rule out such a mechanism in $La_2Fe_4Sb_5$ as it is similarly characterized by geometric frustration in the Fe-sublattice and a large γ. However, here we observe a spin glass like ordering unlike what was observed in LiV_2O_4 making the mechanism for the large linear-in-*T* contribution to $C(T)$ more likely to be magnetic in origin. The anomalously large linear-in-*T* $C(T)$ observed in some spin glass materials is thought to arise from the disruptions of RKKY magnetic interactions between magnetic atoms by a nonmagnetic atom disorder. It is plausible that the enhanced γ that we infer for $La_2Fe_4Sb_5$ results from the disruption of the magnetic interactions within the Fe-sublattice by the Fe2 positional disorder and occupational disorder of the nonmagnetic Sb3 atoms.[46] It would be interesting to study the role of disorder in $La_2Fe_4Sb_5$ and the remaining analogues by varying synthetic conditions, as the degree of disorder greatly affects to glassy behavior of materials. Thus, these experiments would most likely affect the spin-glass behavior observed in the physical properties of $La_2Fe_4Sb_5$ and the other analogues, and provide more insight into the magnetic ordering mechanism for $Ln_2Fe_4Sb_5$ (Ln = La−Nd and Sm) as well as the enhanced Sommerfeld coefficient for $La_2Fe_4Sb_5$.

ASSOCIATED CONTENT

Supporting Information

The Crystallographic Information Files (CIFs) for $Ln_2Fe_4Sb_5$ (Ln = La−Nd and Sm) are provided. This material is available free of charge via the Internet at http://pubs.acs.org.

AUTHOR INFORMATION

Corresponding Author

*E-mail: jchan@lsu.edu. Telephone: (225) 578-2695. Fax: (225) 578-3458.

Notes

The authors declare no competing financial interest.

ACKNOWLEDGMENTS

J.F.D., E.M., and J.Y.C. acknowledge partial support for this work from the National Science Foundation (NSF) through DMR1206763, DMR0847681, and DMR1063735, respectively. W.A.P., J.F.D., and J.Y.C. acknowledge Prof. David P. Young and Dr. Frank Fronczek for useful discussions.

REFERENCES

(1) Macaluso, R. T.; Wells, D. M.; Sykora, R. E.; Albrecht-Schmitt, T. E.; Mar, A.; Nakatsuji, S.; Lee, H.; Fisk, Z.; Chan, J. Y. *J. Solid State Chem.* **2004**, *177*, 293−298.

(2) Thomas, E. L.; Macaluso, R. T.; Lee, H. O.; Fisk, Z.; Chan, J. Y. *J. Solid State Chem.* **2004**, *177*, 4228−4236.

(3) Thomas, E. L.; Gautreaux, D. P.; Chan, J. Y. *Acta Crystallogr., Sect. E: Struct. Rep.* **2006**, *62*, I96−I98.

(4) Thomas, E. L.; Gautreaux, D. P.; Lee, H. O.; Fisk, Z.; Chan, J. Y. *Inorg. Chem.* **2007**, *46*, 3010−3016.
(5) Gautreaux, D. P.; Capan, C.; DiTusa, J. F.; Young, D. P.; Chan, J. Y. *J. Solid State Chem.* **2008**, *181*, 1977−1982.
(6) Gautreaux, D. P.; Parent, M.; Moldovan, M.; Young, D. P.; Chan, J. Y. *Phys. B* **2008**, *403*, 1005−1006.
(7) Phelan, W. A.; Nguyen, G. V.; Karki, A. B.; Young, D. P.; Chan, J. Y. *Dalton Trans.* **2010**, *39*, 6403−6409.
(8) Phelan, W. A.; Menard, M. C.; Kangas, M. J.; McCandless, G. T.; Drake, B. L.; Chan, J. Y. *Chem. Mater.* **2012**, *24*, 409−420.
(9) Drake, B. L.; Grandjean, F.; Kangas, M. J.; Okudzeto, E. K.; Karki, A. B.; Sougrati, M. T.; Young, D. P.; Long, G. J.; Chan, J. Y. *Inorg. Chem.* **2010**, *49*, 445−456.
(10) Lynn, J. W.; Dai, P. *Phys. C* **2009**, *469*, 469−476.
(11) Canfield, P. C. *Nat. Mater.* **2011**, *10*, 259−261.
(12) Zhao, L. L.; Yi, T.; Fettinger, J. C.; Kauzlarich, S. M.; Morosan, E. *Phys. Rev. B* **2009**, *80*, 020404(R).
(13) Todorov, I.; Chung, D. Y.; Malliakas, C. D.; Li, Q. a.; Bakas, T.; Douvalis, A.; Trimarchi, G.; Gray, K.; Mitchell, J. F.; Freeman, A. J.; Kanatzidis, M. G. *J. Am. Chem. Soc.* **2009**, *131*, 5405−5407.
(14) Yi, T.; Dioguardi, A. P.; Klavins, P.; Curro, N. J.; Zhao, L. L.; Morosan, E.; Kauzlarich, S. M. *Eur. J. Inorg. Chem.* **2011**, 3920−3925.
(15) Nambu, Y.; Zhao, L. L.; Morosan, E.; Kim, K.; Kotliar, G.; Zajdel, P.; Green, M. A.; Ratcliff, W.; Rodriguez-Rivera, J. A.; Broholm, C. *Phys. Rev. Lett.* **2011**, *106*, 037201.
(16) Manuel, P.; Chapon, L. C.; Todorov, I. S.; Chung, D. Y.; Castellan, J. P.; Rosenkranz, S.; Osborn, R.; Toledano, P.; Kanatzidis, M. G. *Phys. Rev. B* **2010**, *81*, 184402.
(17) Zhao, L. L.; Kim, S. K.; McCandless, G. T.; Torikachvili, M. S.; Canfield, P. C.; Chan, J. Y.; Morosan, E. *Phys. Rev. B* **2011**, *84*, 104444.
(18) Nakatsuji, S.; Nambu, Y.; Tonomura, H.; Sakai, O.; Jonas, S.; Broholm, C.; Tsunetsugu, H.; Qiu, Y. M.; Maeno, Y. *Science* **2005**, *309*, 1697−1700.
(19) Menard, M. C.; Ishii, R.; Higo, T.; Nishibori, E.; Sawa, H.; Nakatsuji, S.; Chan, J. Y. *Chem. Mater.* **2011**, *23*, 3086−3094.
(20) Nakatsuji, S.; Tonomura, H.; Onuma, K.; Nambu, Y.; Sakai, O.; Maeno, Y.; Macaluso, R. T.; Chan, J. Y. *Phys. Rev. Lett.* **2007**, *99*, 157203.
(21) Woll, P. Ph.D. Dissertation, Technischen Hochschule Darmstadt, 1987.
(22) Altomare, A.; Burla, M. C.; Camalli, M.; Cascarano, G. L.; Giacovazzo, C.; Guagliardi, A.; Moliterni, A. G. G.; Polidori, G.; Spagna, R. *J. Appl. Crystallogr.* **1999**, *32*, 115−119.
(23) Sheldrick, G. M. *Acta Crystallogr., A* **2008**, *64*, 112−122.
(24) Otwinowski, Z.; Minor, W. In *Methods in Enzymology*; Carter, C. W., Jr, Sweet, R. M., Eds.; Academic Press: New York, 1997; Vol. *276*, Macromolecular Crystallography, Part A, pp 307−326.
(25) Nasir, N.; Grytsiv, A.; Rogl, P.; Kaczorowski, D.; Effenberger, H. S. *Intermetallics* **2010**, *18*, 2361−2376.
(26) Acatrinei, A. I.; Browne, D.; Losovyj, Y. B.; Young, D. P.; Moldovan, M.; Chan, J. Y.; Sprunger, P. T.; Kurtz, R. L. *J. Phys. Condens. Matter* **2003**, *15*, L511−L517.
(27) Young, D. P.; Goodrich, R. G.; Ditusa, J. F.; Guo, S.; Adams, P. W.; Chan, J. Y.; Hall, D. *Appl. Phys. Lett.* **2003**, *82*, 3713−3715.
(28) Hartjes, K.; Jeitschko, W.; Brylak, M. *J. Magn. Magn. Mater.* **1997**, *173*, 109−116.
(29) Sefat, A. S.; Bud'ko, S. L.; Canfield, P. C. *J. Magn. Magn. Mater.* **2008**, *320*, 120−141.
(30) Kamihara, Y.; Hiramatsu, H.; Hirano, M.; Kawamura, R.; Yanagi, H.; Kamiya, T.; Hosono, H. *J. Am. Chem. Soc.* **2006**, *128*, 10012−10013.
(31) Takahashi, H.; Igawa, K.; Arii, K.; Kamihara, Y.; Hirano, M.; Hosono, H. *Nature* **2008**, *453*, 376−378.
(32) Thomas, E. L.; Moldovan, M.; Young, D. P.; Chan, J. Y. *Chem. Mater.* **2005**, *17*, 5810−5816.
(33) Holseth, H.; Kjekshus, A. *Acta Chem. Scand.* **1969**, *23*, 3043−3050.
(34) Holseth, H.; Kjekshus, A.; Andresen, A. F. *Acta Chem. Scand.* **1970**, *24*, 3309−3316.
(35) Ramirez, A. P. *Annu. Rev. Mater. Sci.* **1994**, *24*, 453−480.
(36) Kleinke, H.; Ruckert, C.; Felser, C. *Eur. J. Inorg. Chem.* **2000**, *31*, 315−322.
(37) Papoian, G. A.; Hoffmann, R. *Angew. Chem., Int. Ed.* **2000**, *39*, 2409−2448.
(38) Mills, A. M.; Lam, R.; Ferguson, M. J.; Deakin, L.; Mar, A. *Coordin. Chem. Rev.* **2002**, *233*−*234*, 207−222.
(39) Eisenmann, B. *Z. Naturforsch. B* **1979**, *34*, 1162−1164.
(40) Chan, J. Y.; Wang, M. E.; Rehr, A.; Kauzlarich, S. M.; Webb, D. J. *Chem. Mater.* **1997**, *9*, 2131−2138.
(41) Gersten, J. I.; Smith, F. W. *The Physics and Chemistry of Materials*; John Wiley: New York, 2001; pp xxix, 826.
(42) Mydosh, J. A. *Phys. Rev. Lett.* **1974**, *33*, 1562−1566.
(43) Rauchschwalbe, U.; Steglich, F.; Rietschel, H. *Phys. B & C* **1987**, *148*, 33−36.
(44) Fisk, Z.; Sarrao, J. L.; Smith, J. L.; Thompson, J. D. *Proc. Natl. Acad. Sci. U.S.A.* **1995**, *92*, 6663−6667.
(45) Johnston, D. C. *Phys. B* **2000**, *281*−*282*, 21−25.
(46) Gschneidner, K. A.; Tang, J.; Dhar, S. K.; Goldman, A. *Phys. B* **1990**, *163*, 507−510.